ECS Transactions

The Electrochemical Society
Advancing solid state & electrochemical science & technology

Material and Design Options for Avoiding Lithium Plating during Charging

To cite this article: Kevin Eberman *et al* 2010 *ECS Trans.* **25** 47

View the article online for updates and enhancements.

You may also like

- Coupling Lithium Plating with SEI Formation in a Pseudo-3D Model: A Comprehensive Approach to Describe Aging in Lithium-Ion Cells
Serena Carelli and Wolfgang G. Bessler

- Nonlinear harmonic excitations in collisional, asymmetrically-driven capacitive discharges
Jian-Kai Liu, Emi Kawamura, Michael A Lieberman et al.

- Effects of the transverse electric field on nanosecond pulsed dielectric barrier discharge in atmospheric airflow
Yongfeng XU, , Hongfei GUO et al.

This content was downloaded from IP address 54.68.131.140 on 05/12/2024 at 16:37

Zhuhai CosMX Battery Co. - EX1022
Zhuhai CosMX Battery Co. v. Ningde Amperex Tech. Ltd.

ECS Transactions, 25 (35) 47-58 (2010)
10.1149/1.3414003 ©The Electrochemical Society

Material and Design Options for Avoiding Lithium-Plating during Charging

Kevin Eberman, Parthasarathy M. Gomadam, Gaurav Jain and Erik Scott

Medtronic Energy and Component Center, Brooklyn Center, Minnesota 55311, USA

A two-dimensional model is presented, including the thickness and electrode edge-overlap directions, which successfully predicts the onset of lithium plating observed experimentally with carbon negative electrodes under certain conditions. Plating with $Li_4Ti_5O_{12}$ (about 1.5 V vs lithium) did not occur experimentally, nor was it predicted by the model over a wide parameter window up to 5C. High charge rate (e.g. up to 5C) with up to 1.7mm "underlap" (positive-electrode edge extending beyond that of the negative-electrode) can be accomplished with a negative-electrode open-circuit potential above 0.4V vs. carbon.

Introduction

In lithium ion batteries, an important design objective is to avoid the plating of lithium during charging. Generally, plated Li is not completely reversible, and therefore even small amounts can have significant consequences due to accumulation with cycling. The consequences can include loss of capacity, mechanical swelling and, potentially, the formation of an electrical short. Cell design aspects commonly applied to avoid lithium-plating include cell balance (areal capacity ratio of the negative electrode to that of the positive), electrolyte fill, current and "overlap" (the distance by which the negative electrode extends beyond the edge of the positive electrode, Fig. 1).

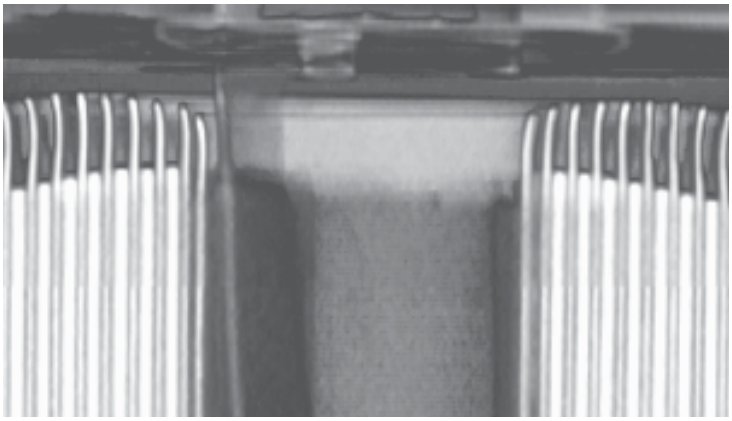

Figure 1. X-ray computed tomograph of upper portion of cylindrically wound cell, illustrating edge overlap of negative electrode beyond the positive electrode. In this cross sectional view of concentric windings of the coil, the negative electrode's overlapped edges appear as a comb-like structure. (Image courtesy of Exponent Inc.).

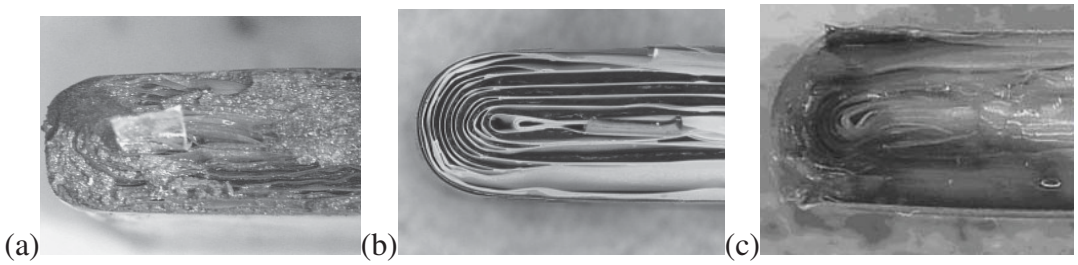

Figure 2. Top edges of three heavily cycled experimental Li-ion coils: (a) $LiCoO_2$||C cell with zero overlap, (b) $LiCoO_2$||$Li_4Ti_5O_{12}$ cell with zero overlap, (c) $LiCoO_2$||C cell with >1mm overlap. Only (a) shows Li-plating.

Lithium-plating is not expected as long as the potential of the negative electrode is maintained above 0 V (versus Li/Li+). However, in practice lithium-plating can be induced even when the apparent negative electrode potential, as measured versus a reference electrode in the cell, is well above 0 V. This is because local electrochemical potentials in the porous electrode can vary greatly under dynamic conditions, in some cases, by several hundred mV even at moderate currents [1]. The potential variation across the plane of the electrode surface can be detected in situ through careful placement of sufficiently small reference electrodes. However, regarding the variation perpendicular to the electrode plane (such as within a thick porous electrode), in situ methods may not be practical. Two-dimensional mathematical modeling offers a useful way to study potential variations in both directions, as recently shown by Newman's group [2].

The choice of negative electrode active material can profoundly reduce the likelihood of lithium plating. Most prominent is the potential at which Li+ ions are inserted during charging, but relative reaction kinetics and mass transfer rates at the electrodes are also operative.

In this paper, we present modeling and experimental studies of the effects of design and use-dependent parameters on Li-plating. We present results comparing graphite, which inserts Li+ down to approx. 0.05 V, to $Li_4Ti_5O_{12}$, which inserts Li+ down to about 1.5 V. We make predictions of potential variations in electrodes of various active materials with a range of Li inserting potentials, kinetic parameters, and cell designs to determine the best materials for given applications. We show the limits of electrode underlap, deposition, and density for preventing Li-plating. We show that $Li_4Ti_5O_{12}$ active material provides a much broader cell design space for avoiding lithium-plating. (Fig. 2).

Experiment and Modeling

Experiment

Optical cells were constructed for viewing the electrodes during charge and discharge. The stainless steel cells were equipped with feed-throughs for the positive and negative electrodes, a fill port that was sealed by a Swagelock™ fitting and a sapphire window. Fig. 3 below shows schematic cross sections which illustrate how the two cells of this experiment were designed. The first (Fig. 3(a)) was designed to create an extreme condition in order to view extensive plating. The graphite negative-electrode was coated on both sides of a perforated current collector, so that the extent of the Li + C reaction could be observed across the entire electrode as the lithium plated on the circumference

(Fig. 4). The second (Fig. 3(b)) was designed to use electrodes that were configured in a manner to more closely simulate the repeating unit of a cell stack in commercial cells. The repeat unit consisted of a sandwiched stack of the following layers: foil positive current collector with $LiCoO_2$ coating, microporous separator; negative active coating on a foil current collector. Exposed areas of bare metal on the back-sides of the electrodes were avoided by application of a layer of electrolyte-compatible adhesive tape.

The two cells of this type employed a 3 mAh/cm^2 LCO ($LiCoO_2$) positive electrode, a 20 micron Celgard 2320 separator, and 1M $LiPF_6$ electrolyte. All electrodes were about 30% porous and about 90wt% active. The areal-capacity ratios, Q_N/Q_P, were 1.1 and 0.7 for the MCMB and $Li_4Ti_5O_{12}$ cells respectively. Constant current followed by constant voltage charging was used for both.

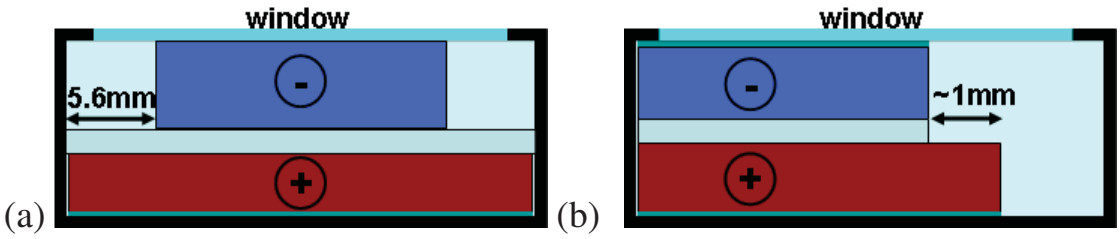

Figure 3. Schematic representations of the Optical Cell cross section. A microscope was used to collect images from above through a sapphire window in the top of the cell, such that the separator and positive-electrode were behind the negative-electrode. (a) Cell used to study gross plating: MCMB || LCO cell. Both electrodes were circular. (b) Design used for comparing ~1mm underlap for MCMB || LCO and for LTO ||LCO to the model. Both electrodes were approximately semi-circular.

1-D Model

The model for Li-ion batteries presented in Ref. [3] and [4] is adapted to develop a 1-D model for Medtronic's Li-ion battery of $LiC_6/LiCoO_2$ chemistry. The model equations are summarized in Fig. 8. The model is validated against experimental data for various rates of charge and discharge. Table 1 shows model parameters and their values, some of which were estimated using the fitting routine followed in Ref. [3]. Voltage curves obtained experimentally at a rate of C/24 were used as OCVs for the two electrodes. Concentration-dependent electrolyte conductivity, diffusion coefficient and transference number, used to improve model predictions at higher rates, have been published previously [5]. The comparison between model predictions and experimental data during charging are shown in Fig. 4. Overall, the 1-D model predicts voltages well, although the error in the model increases with rate.

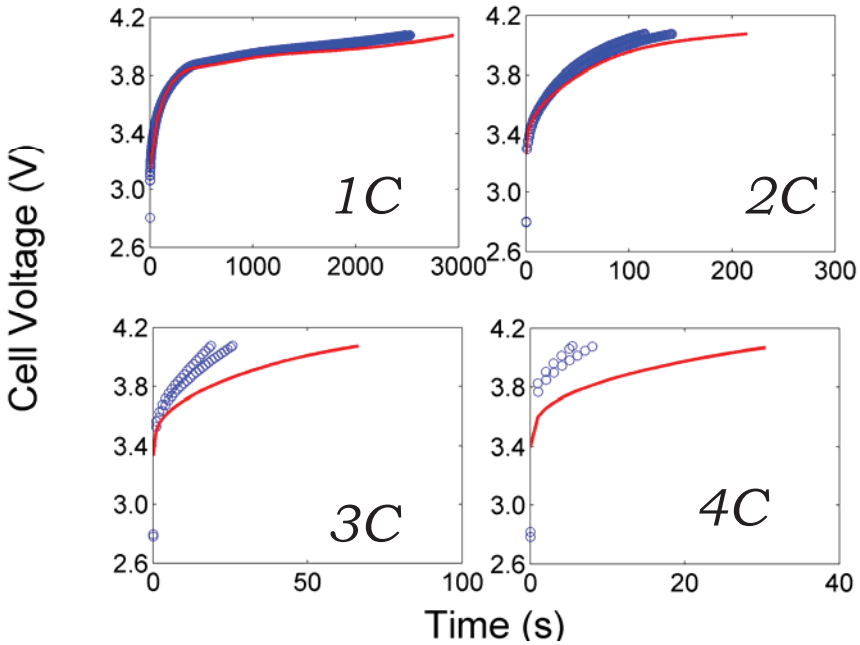

Figure 4. Model (line) vs. data (circles) at various charge rates. The model predictions at rates less than 1C are as good or better than at 1C.

2-D Model Approach

The optical cell described in Fig 3(b) is modeled to evaluate conditions for Li plating. Following the approach of Ref. [5], the 1-D model equations presented above were extended to 2-D. A schematic perspective of the optical cell is shown in Fig 5. The region of interest is two-dimensional, encompassing the two electrodes, the current collectors, the separator, and the free electrolyte. The interfaces between these cell components, along with the black dotted lines, divide the solution domain into 15 sub-domains. For reasons of model accuracy and flexibility, each sub-domain is scaled to a unit square. The model equations in the two dimensions are also scaled accordingly.

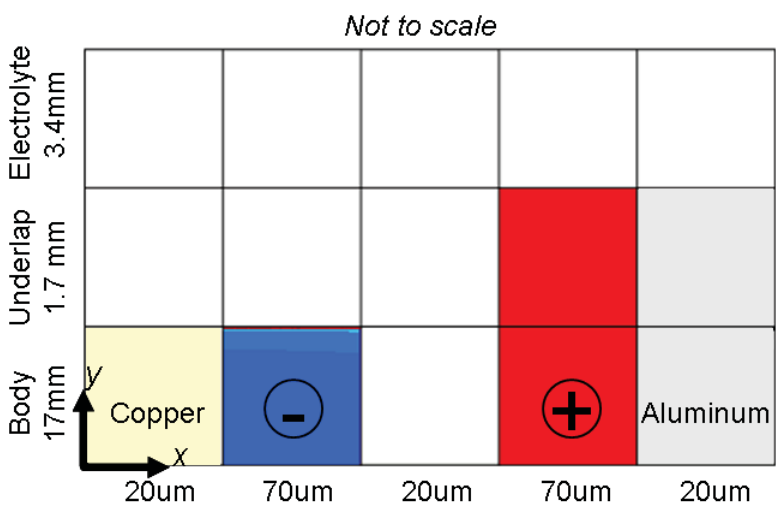

Figure 5. Solution domain with 15 sub-domains, each scaled to a unit square.

The 2-D model is solved for various rates of charging from a fully discharged state. The calculated potentials and concentrations at each point in the solution domain are used to calculate the local overpotential for Li plating as

$$\eta_{Li} = \phi_1 - \phi_2 - \frac{RT}{F}\ln\left(\frac{c}{c^0}\right) \qquad [1]$$

The condition for Li plating is: $\eta_{Li} \leq 0\,\mathrm{V}$.

The model is used to evaluate the effect of geometrical parameters such as underlap, and material properties such as the exchange-current density. Further, the effect of using hypothetical negative electrode materials of various open-circuit voltages is evaluated. The various negative electrode materials are represented in the model by varying an additive term to U_N. Graphically, this amounts to vertically displacing the OCV curve of carbon, keeping the same θ-dependency.

Results and Discussion

In-situ observation of lithium plating: First we present an example of experimental observation of lithium plating using the optical cell described in Fig. 3(a). This MCMB || LCO cell was built with an exaggerated underlap. (Note that we are not aware of cell designs that include intentional underlap. However, depending on design and processing conditions, an underlap condition may occur in some region of a cell, if dimensional and alignment tolerances are not adequately managed.) The cells were cycled at increasing rates and various representative images are shown in Fig. 6. Notably, gross lithium plating occurred on the edge well before the electrode has fully reacted to the gold LiC_6 phase (Fig. 6(a)). At the end of discharge, some of the plated lithium is consumed; however, some is left behind and is rendered inactive (Fig. 6(b)). Even a discharge to zero volts (full cell) did not consume this "lost" lithium, and by the fourth discharge an even greater quantity of lithium has been lost (Fig. 6(d)). This "lost" lithium appears to be in direct contact with the graphite electrode, but we infer that it must be electrically isolated, due to its persistence during cell discharge. A possible cause of isolation is the formation of an insulating layer on the surface of lithium due to irreversible reaction with the electrolyte. The permanent isolation of lithium represents one type of capacity fade for lithium-ion cells.

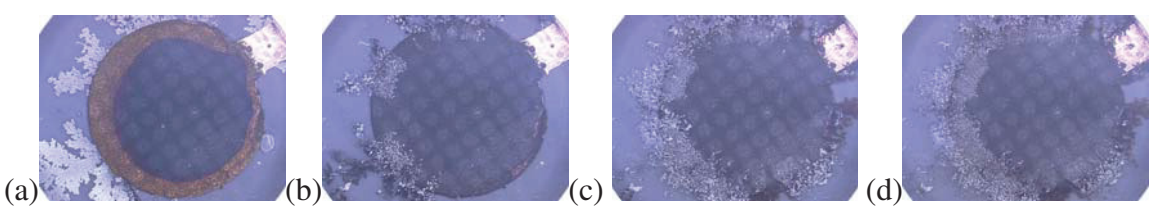

Figure 6. Images from MCMB || LCO Optical Cell showing plating and lost lithium during cycling: (a) Top of 1st charge at C/10, (b) Bottom of 1st discharge at C/2, (c) Bottom of 3rd discharge at C/10 to zero volts, (d) bottom of 4th discharge at C/2, followed 20 hours open circuit. The dark round disk in each image is the negative electrode, and underneath it behind the separator is the positive electrode, 5.6 mm greater in radius (Fig.3(a)). The fractal-like lighter colored regions are lithium which forms during charging, and some of which persists even with subsequent discharge. The lighter region

forming the outer ring in the negative electrode in (a) and (c) is the fully lithiated gold-phase, i.e., LiC_6.

Validation of 2-D model: With this optical cell set-up in place, we conducted experiments to validate predictions of the 2-D model described above. We built MCMB||LCO and LTO||LCO cells, similar to those described in Fig. 3(b), with a target underlap of 1 mm. After assembly, the underlap dimensions were 1.7 mm and 0.5 mm for the MCMB||LCO and LTO||LCO cells, respectively. The cells were then charged at increasing rates, while monitoring the state-of-charge (SOC) at the onset of lithium plating. This was then compared to the model predictions. The model output model was the SOC at which the local overpotential of plating (η_{Li}) first became <0 (indicative of onset of Li plating). For the MCMB || LCO cell the model predicted onset of lithium plating for this experimental set-up at 11% SOC when charging at C/10. In our optical cell, the first specs of lithium were observed at 6% SOC. This shows close initial agreement between the model and data.

For the LTO || LCO cell, the model predicts that lithium plating does not occur, even when the charge rate is increased up to 5C. The optical cell confirms this result. This reinforces the intrinsic plating resistance of cells with lithium titanate negative active material; even with cells built with exaggerated underlap, and at extreme charge rates, no lithium plating is observed. Furthermore, the lack of lithium plating with LTO || LCO cells eliminates "lost" lithium as a mechanism for capacity fade, thus offering more stable capacity with cycling.

It is worth pointing out two unique observations regarding lithium plating made through these optical cell measurements. First, the maximum extent of lithium plating may not be observed when a cell is destructively analyzed, unless the analysis is undertaken promptly after charge. Also, it is important to note that while plated lithium is commonly mentioned as causing a shorting risk, no shorts were noted in these experiments. The dendrites apparently do not readily penetrate the separator and can become electrically isolated, and thus don't always cause a short.

Predictions with the model: As highlighted earlier, numerous factors affect lithium plating. These include thermodynamic parameters such as negative electrode open circuit potential; kinetic parameters such as exchange current density across the negative electrode / electrolyte interface, Li^+ diffusion coefficients in the negative electrode solid phase, and Li^+ diffusion in the electrolyte; and cell design and operational parameters such as cell balance, electrode underlap, electrode porosities and charge rate. Because the number of materials available is finite, and because any given material has a bundled set of properties, it is not possible to experimentally evaluate the effects of all of these factors on plating in an orthogonal and comprehensive manner. However, using the 2-D model, we conducted a sensitivity analysis, in which each of these factors was varied over a pre-specified range and the effect on the risk of lithium plating was quantified. Table 2 lists the factors, the range over which they were varied and the direction and relative magnitude of effect on lithium plating, in decreasing order.

Table 1. Sensitivity analysis of materials, design and operational parameters on lithium plating. Factors are listed in order from greatest to least magnitude of effect (indicated by boldness of the arrow), and arrows indicate direction of effect. For example, increasing the negative-electrode open-circuit potential from 0 to 1.5V greatly reduced the risk of Li plating.

By Increasing Parameter	Symbol	Range	Risk
Negative Open-Circuit Potential	U_N	0 to 1.5 V	↘
Underlap	y_u	0.017 to 1.7 mm	↗
Charge Rate	I_{app}	C/10 to 5C	↗
Negative:Postive Ratio	Q_N / Q_P	1.0 to 1.2	↘
Exchange Current Density	$i_{o,N}$	0.1 to 100 A/m^2	↘
Negative Diffusion Coefficient	D_N	10^{-10} to 10^{-9} m^2/s	↘
Deposition (porosity constant)		1 to 3 mAh/cm^2	↘
Porosity (deposition constant)		30% to 45%	↘
Initial Salt Concentration	c^o	1 to 2 M	↗

The sensitivity analysis shows the negative electrode open circuit potential has the strongest effect on reducing the risk of lithium plating. Interestingly, over the specified range of the various factors, electrode underlap and charge rate have stronger effects than negative/positive capacity ratio. Regarding exchange current density, even with a large variation range, the effect is relatively small. The negative electrode diffusion coefficient was varied over a relatively short range and turn out to have a small effect. Increasing deposition, which manifests as a thicker electrode, lowers the risk of plating by lowering the flux from the overlapping portion of the positive at any point along the thickness. Increasing porosity lowers the risk in two ways; 1) by providing a thicker electrode at a given capacity loading; and 2) by making Li^+ transport in the electrolyte faster. Increasing the salt concentration increases the risk of plating.

Eliminating the risk of lithium plating: With the three top factors determined from the sensitivity analysis, we once again employed the 2-D model to conduct experiments at three levels for each factor. The other variables such as cell balance, exchange current density and so forth were held constant at experimentally validated values (Appendix). To represent three levels of negative electrode open circuit potential we chose the MCMB voltage curve and translated it to a higher voltage by adding 0V, 0.2V and 0.4V. Underlap levels of 0.017 mm, 0.17 mm and 1.7 mm and charge rates of C/10, 2C and 5C were probed as the other two factors. The results from this experiment are shown in Fig. 7. Although the model predicts precisely the SOC for onset of lithium plating, here we present only the key result: whether lithium plating occurs or not (through full charge) for a given set of inputs. At C/10, lithium plating is predicted only when the underlap is >0.17 mm and the negative OCP is <0.2V; at other levels, no lithium plating is observed at this current. At 2C and at 5C, lithium plating is predicted for >0.017 mm underlap for negative OCP < 0.4V. This validates the common practice that for cell designs with graphite as the negative electrode, avoiding electrode underlap

is important to avoid lithium plating. Notably, for negative OCP > 0.4V, lithium plating is not predicted for any underlap.

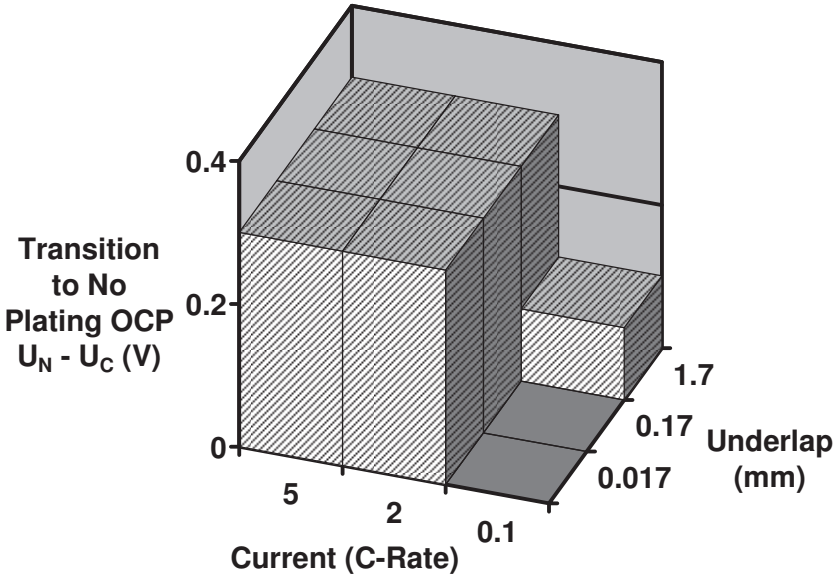

Figure 7. Column chart shows the approximate level of the negative-electrode open circuit potential (above that of graphite) for the transition from a non-plating to a plating condition given the charge rate and the underlap.

Based on the results from the 2-D model presented here, materials with an OCP of ≥0.4 V vs MCMB are of attractive to minimize plating risk during rapid recharge. Another benefit of such materials would be lower reactivity with the electrolyte. This would reduce the criticality of the SEI, allow new electrolyte formulations and offer cells without the increased irreversible capacity, fade and impedance associated with the SEI. Materials that fall within this realm possibly include: alloy negatives, hard-carbons, and certain transition metal oxides.

Conclusions

The 2-dimensional model presented, including the thickness and electrode edge-overlap directions, successfully predicted the onset of plating observed experimentally. Plating with $Li_4Ti_5O_{12}$ did not occur in the model over a wide parameter window up to 5C, and was not observed experimentally. High charge rate (e.g. 2C, 5C) with 1.7 mm underlap can be accomplished with a negative-electrode open-circuit potential 0.4V above that of carbon. Even at the carbon open-circuit potential, plating was not seen in the model at a low charge rate of C/10 with up to 0.17mm of underlap.

Appendix

	Negative Electrode	Separator	Positive Electrode	
	Charge Balance	Charge Balance	Charge Balance	
$\phi_1 = 0$	$\sigma_N \frac{\partial^2 \phi_1}{\partial x^2} = j$	–	$\sigma_P \frac{\partial^2 \phi_1}{\partial x^2} = j$	$\phi_1 = E$
$\frac{\partial \phi_2}{\partial x} = 0$	$\frac{\partial}{\partial x}\left(\kappa_N \frac{\partial \phi_2}{\partial x} + \kappa_N^D \frac{\partial \ln c}{\partial x}\right) = -j$	$\frac{\partial}{\partial x}\left(\kappa_S \frac{\partial \phi_2}{\partial x} + \kappa_S^D \frac{\partial \ln c}{\partial x}\right) = 0$	$\frac{\partial}{\partial x}\left(\kappa_P \frac{\partial \phi_2}{\partial x} + \kappa_P^D \frac{\partial \ln c}{\partial x}\right) = -j$	$\frac{\partial \phi_2}{\partial x} = 0$
	Material Balance	Material Balance	Material Balance	
	$\frac{\partial \theta_N}{\partial t} = \frac{D_N}{r^2}\frac{\partial}{\partial r}\left(r^2 \frac{\partial \theta_N}{\partial r}\right)$ $-D_N \left.\frac{\partial \theta_N}{\partial r}\right\|_{r=R_N} = \frac{j}{n_N F c_{1,N}^{max}}$	–	$\frac{\partial \theta_P}{\partial t} = \frac{D_P}{r^2}\frac{\partial}{\partial r}\left(r^2 \frac{\partial \theta_P}{\partial r}\right)$ $-D_P \left.\frac{\partial \theta_P}{\partial r}\right\|_{r=R_P} = \frac{j}{n_P F c_{1,P}^{max}}$	
$\frac{\partial c}{\partial x} = 0$	$\varepsilon_N \frac{\partial c}{\partial t} = \varepsilon_N^{p_N} D \frac{\partial^2 c}{\partial x^2} + \frac{\left(1 - t_+^0\right) j}{F}$	$\varepsilon_S \frac{\partial c}{\partial t} = \varepsilon_S^{p_S} D \frac{\partial^2 c}{\partial x^2}$	$\varepsilon_P \frac{\partial c}{\partial t} = \varepsilon_P^{p_P} D \frac{\partial^2 c}{\partial x^2} + \frac{\left(1 - t_+^0\right) j}{F}$	$\frac{\partial c}{\partial x} = 0$

$$\kappa = \kappa^{free} \varepsilon^p \qquad \kappa^D = -\kappa \frac{2\left(1 - t_+^0\right)}{f} \qquad j = a i_0 \left(e^{\beta f \eta} - e^{-(1-\beta) f \eta}\right) \qquad \eta = \phi_1 - \phi_2 - U$$

Figure 8. Summary of model equations.

Table 2. Model parameters

Parameter	Value	Source
A	137.8 cm^2	Design
$c_{1,N}^{max}$	30555.56	Stoichiometry
$c_{1,P}^{max}$	51554.19	Stoichiometry
L_N	74.66 µm	Design
L_S	40 µm	Design
L_P	71.56 µm	Design
c_2	1 M	Design
k_N	1.5 x 10^{-6}	Estimated
k_P	1.5 x 10^{-6}	Estimated
n_N	1	Stoichiometry
n_P	1	Stoichiometry
p_N	2.5	Estimated
p_S	2.4	Design
p_P	2.5	Estimated
R_{fN}	0	Assumed
R_{fP}	0	Assumed
R_N	30 µm	Design
R_P	10 µm	Design
$\alpha_{a,N}$	0.5	Assumed
$\alpha_{c,N}$	0.5	Assumed
$\alpha_{a,P}$	0.5	Assumed
$\alpha_{c,P}$	0.5	Assumed
$\varepsilon_{e,N}$	0.5629	Design
$\varepsilon_{e,P}$	0.5489	Design
ε_N	0.3418	Design
ε_S	0.41	Design
ε_P	0.3023	Design
κ^{free}	9.64 mS/cm	Design
θ_N^0	0.002	Estimated
θ_P^0	0.88	Estimated
σ_N^{free}	1 S/cm	Assumed
σ_P^{free}	1 S/cm	Assumed

List of Symbols.

a	Specific surface area of electrode, cm^2/cm^3
A	Geometric area of electrode, cm^2
c	Concentration, mol/cm^3
D	Electrolyte diffusion coefficient, cm^2/s
D_N, D_P	Li diffusion coefficient in negative and positive particles, cm^2/s
E	Cell voltage, V
f	Constant, 37.44 V^{-1}
F	Constant, 96487 C/mol
i_0	Exchange-current density, A/cm^2
I_{app}	Cell current, A
j	Local volumetric reaction current density, A/cm^3
k	Rate-constant, A/cm^2
L	Thickness, cm
n	Number of electron transferred
p	Bruggeman exponent
R	Particle radius, cm
t	Time, s
t_+^0	Li^+ transference number in electrolyte
U	Open-circuit potential, V
x	Position, cm

Greek

α	Transfer-coefficient
ϕ	Local potential
ε	Porosity
ε_e	Volume-fraction of active material
κ	Ionic conductivity, S/cm
θ	Lithiation level
σ	Electronic conductivity, S/cm

Subscript

1	Solid phase
2	Solution phase
a	Anodic
c	Cathodic
N	Negative electrode
S	Separator
P	Positive electrode

Superscript

0	Initial
free	Free form
DL	Delithiation
L	Lithiation
max	Maximum

References

1. E. Scott, G. Tam, B. Anderson and C. Schmidt, Paper 1282 presented at the Electrochemical Society meeting, Orlando, FL, October 13, 2003.
2. M. Tang, P. Albertus, and J. Newman, *J. Electrochem. Soc.*, **156** (5) A390-A399 (2009).
3. T. Fuller, M. Doyle, and J. Newman, *J. Electrochem Soc.*, **141**, 1 (1994).
4. M.Doyle, J.Newman, A.S.Gozdz, C.N.Schmutz, and J-M.Tarascon, *J. Electrochem. Soc.*, **143**, 1893 (1996).
5. K. Gering, *Electrochim. Acta*, **51**, 3125 (2006).